 DOI: 10.1002/masy.201251003

Fabrication of Bioactive Polyoxymethylene Nanocomposites for Bone Tissue Replacement

Ajith James Jose,[1,2] *M. Alagar**[1]

Summary: Stearic acid modified nano hydroxyapatite (n-SHA) filled polyoxymethylene (POM) nanocomposites were prepared by melt mixing method for bone tissue replacement and regeneration applications. Contact angle measurements of POM nanocomposites were carried out to understand the effect of n-SHA addition on the hydrophobicity of nanocomposites. The mechanical properties like tensile strength, Young's modulus and elongation at break were found to be increased significantly by the incorporation of n-SHA into the POM matrix. The bone-bonding ability of the nanocomposites was evaluated by examining the apatite formation on their surface after soaking in simulated body fluid (SBF) and apatite formation was studied by atomic force microscopy (AFM). The protein adhesion studies revealed the enhanced biocompatibility of the nanocomposites due to the presence of n-SHA nanofillers on the surface and it provides favorable binding sites for protein adsorption. The significant improvement in the biocompatibility as well as mechanical, thermal and hydrophobic properties of the POM nanocomposites makes it a potential future material for bone implantation.

Keywords: biocompatibility; hydrophobicity; mechanical properties; nanocomposites; polyoxymethylene

Introduction

In view of the growing number of traffic accidents and human life expectancy, bone is emerged as the most frequently transplanted human tissue and its demand is growing in medical market for reconstruction of bone defects.[1] Current methods of broken and defective bone treatment use metal orthopedic implants, unfortunately shows many shortcomings such as insufficient prolonged bonding between the implanted material and juxtaposed bone, difference in mechanical properties between bone and the implant leading to stress shielding, release of certain ions and corrosion products from metallic implants and the need of second surgery to remove the implant.[2] So researchers in the field of orthopedics have given considerable emphasis on the fabrication of reliable and economically feasible biomaterials for bone tissue replacement and regeneration applications.

Among the various bioceramics, hydroxyapatite (HA) is an ideal material to develop bone tissue engineering scaffold due to its osteoconductive and osteoinductive properties as well as the close structural composition to natural bone. But its brittleness and poor performance in terms of mechanical stability limit its use for the regeneration of non-load-bearing bone defects. On the other hand, biocompatible polymers which are widely used in bone grafting also persists some practical difficulties such as low efficiency of cell seeding and poor mechanical property compared with natural hard tissue.[3] Since these currently designed scaffold materials fulfill only part of the requirements, it

[1] Department of Chemical Engineering, Anna University, Chennai- 600 025, India
[2] R & D Centre, Thejo Engineering Limited, Chennai, 600 067 India

remains a great challenge to design an ideal bone graft that emulates natures own structure.

Nanocomposites consist of bioactive polymers and ceramic nanoparticles are considered as the next generation scaffolds for tissue regeneration applications than that of the scaffolds developed by these components individually.[4] The advantages of polymeric biomaterials, compared to metallic or ceramic materials are the ease of manufacturing, availability in various shapes, reasonable cost and superior physical and mechanical properties. Among the biocompatible and bio-stable polymers, polyoxymethylene is a high performance polymer with high strength and stiffness, biological inertness, resiliency, toughness, low friction coefficient and unique long life under sterilization procedures. Due to its bioactive nature and mechanical resistance, POM can be used for joint replacement components and other long-term implants.[5–7] Hydroxyapatite particles have been widely utilized in the fabrication of bone-like hybrid polymer nanocomposites due to its structural and compositional similarity to minerals of natural bones.[8] It can be obtained in nanostructured form, which facilitates the fine dispersion in the polymer matrix and for producing favorable interactions with bioactive polymer and tissue. In particular, these nano-sized components in the polymer matrix provides multiple avenues to engineer implants by tailoring the surface for enhanced interaction with proteins, cells, and apatite nucleation at the same time creating implant materials with better mechanical properties.[9]

The objective of the work is to prepare POM nanocomposite bone implant with integrated bioactivity and physico-chemical properties for bone tissue engineering by combining orthopedics and nanotechnology. Hydroxyapatite nanoparticles (n-HA) prepared by the chemical precipitation method were organically modified with stearic acid (Sa) and characterized using different techniques, such as ATR-FTIR, XRD and TEM. POM nanocomposites with variable amounts of stearic acid modified nano hydroxyapatite (n-SHA) were prepared by melt mixing method and mechanical, hydrophobic, thermal and biocompatible properties were investigated. The morphology of the POM nanocomposites was studied using AFM. The bioactivity of the nanocomposites was evaluated by monitoring the concomitant formation of apatite on the material surface after soaking them in simulated body fluid (SBF). Moreover, the protein adsorption on the nanocomposite surface, which plays a prominent role in attachment and spreading of osteoblast cells, were studied quantitatively by adsorption experiments and qualitatively by AFM imaging and the results are discussed.

Experimental Part

Materials

The polymer matrix used in this study was POM homopolymer (Delrin 501S NC010) purchased from DuPont Company. The melt flow index of POM is 15 g/10 min at 190 °C and density is 1.42 g/cm^3. Calcium nitrate tetra hydrate, trisodium phosphate, stearic acid (SRL, India) and bovine serum albumin (Intergen company) were used as received.

Methods

Preparation of Hydroxyapatite (n-HA) Nanoparticles

Calcium nitrate tetra hydrate and trisodium phosphate were used as calcium and phosphorus precursors for the synthesis of hydroxyapatite nanoparticles using sol–gel precipitation technique. 1 M calcium nitrate solution was added slowly to 0.6 M trisodium phosphate solution with stirring. To this mixture ammonia was added drop wise until the pH of the solution reaches 11, which results in the formation of white precipitate settling at the bottom of the beaker. This precipitated solution was rigorously stirred for 2 h and aged at room temperature for 24 h. The precipitate was separated from the solution using filter paper and washed

repeatedly using warm double distilled water. The product obtained was dried at 60 °C for 24 h in a dry oven. This dried powder was calcined in air at 600 °C for 5 h using an electrical furnace and employing a heating rate of 10 °C/min.

Stearic Acid Modification of n-HA

The prepared nano hydroxyapatite was modified with stearic acid to attain uniform dispersion in the polymer matrix and to increase the interfacial adhesion between organic polymer and inorganic n-HA.[10] At first, 0.7 g of stearic acid was dissolved in100 mL of acetone to form a clear Sa solution. Then 10 g of n-HA powder was added to the Sa solution and the mixture of n-HA/Sa/solvent system was put into a reflux setup. The modified n-HA powders were collected after washed several times by hot ethanol to remove the free Sa adsorbed on the surface and dried at 80 °C for 24 h.

Preparation of Nanocomposites

The POM/n-SHA nanocomposites were prepared by a conventional melt-mixing technique.[11] POM pellets were weighed and put into a twin screw extruder that was preheated up to 190 °C. After those pellets were completely molten at a rotation speed of 30 rpm, the weighed n-SHA was added into the molten POM matrix, and then the POM/n-SHA mixtures were mixed further for 10 min at 190 °C at 90 rpm; such a high rotation speed and long mixing time were essential to obtain a homogeneous dispersion of nanofiller throughout the matrix; subsequently the POM/n-SHA nanocomposites were heated up to 190 °C, molded into a sheet of 1 mm thickness under a pressure of 10 MPa, then cooled down slowly to room temperature. The compositions of the nanofillers used were 0, 1, 3 and 5 percent by weight and the nanocomposites were designated as POM, POM1, POM3, and POM5 respectively.

Characterization of Nanoparticles and Nanocomposites

X-ray diffraction patterns of nanoparticles were taken by a Bruker AXS D8 Advance diffractometer with Cu Kα radiation ($\lambda = 1.5406$ A°). The samples were scanned with a step size of 0.02° in a range of $2\theta = 2°–70°$. ATR-FTIR of n-HA and n-SHA were done using IFS 66 V/S (Bruker) spectrometer with ATR technique with 'Golden Gate' unit in the mid IR region to monitor the interactions between n-HA and Sa. Scans were done in transmission mode from 4000 to 400 cm^{-1}. The TEM images of nanoparticles before and after organomodification were obtained using a transmission electron microscope (JEOL JEM-1011) operated at an accelerated voltage. The samples were prepared by deposition a solution drop in a grid of copper of 300 mesh covered with amorphous carbon.

Tapping mode AFM images of nanocomposites were recorded in ambient atmosphere at room temperature with Nanoscope III (Digital Instruments, Santa Barbara, USA). The probes were commercially available silicon tips with a spring constant of 20–80 N/m, a resonance frequency lying in the 255–300 kHz range. Images were analyzed using a Nanoscope image processing software. The contact angle measurements were carried out by a Goniometer (GBX, France) using sessile drop method. The samples were dried at 60 °C in a vacuum oven for 24 h prior to measurement. A MilliQ grade water drop of 5 μL was slowly and steadily placed on a sample size of 100×100 mm^2, with a micro syringe. The contact angle was measured in air at room temperature within 30 seconds of the addition of water drop and photographs were taken. The average contact angle from at least six different locations on each polymer nanocomposites was determined and the experimental uncertainty was within $\pm 1°$. The tensile properties were investigated using Universal testing machine (UTM, H10KS Tinius Olsen, U.K) at a cross head speed of 10 mm/min with gauge length of 25 mm. Tests were carried out at room temperature using rectangular samples of $10 \times 1.2 \times 0.2$ cm^3 (ASTM D 638). At least five specimens were tested for each set of samples, and the mean values were reported.

From the stress - strain curves the tensile strength, Young's modulus and elongation at break was determined. The TGA analysis was performed in a Universal V4.5A TA DTG analyzer in nitrogen atmosphere to study the systematic weight loss and thus the thermal stability of the specimens. Samples were scanned from room temperature to 600 °C at a heating rate of 10 °C/min.

Biocompatibility Studies

The essential requirement for an artificial material to bond to living bone is the formation of bone like apatite on its surface when implanted in the living body, and this in vivo apatite formation can be reproduced in a simulated body fluid with ion concentrations nearly equal to those of human blood plasma. The SBF was prepared by the procedure proposed by Kokubo et al by dissolving the reagent grade NaCl, $NaHCO_3$, KCl, $K_2HPO_4.3H_2O$, $MgCl_2.6H_2O$, $CaCl_2.2H_2O$ and Na_2SO_4 into distilled water, and buffered with tris (hydroxymethyl-aminomethane, $NH_2C(CH_2OH)_3$) and hydrochloric acid (HCl) to pH 7.4 at 37 °C.[12] After soaking, POM nanocomposites with appropriate size of $1 \times 1\,cm^2$ in SBF for 7 days at 37 °C, samples were removed from SBF, gently washed with deionized water, and dried at room temperature. The surface morphology of the composites after soaking in SBF solutions was characterized using AFM to confirm the formation of apatite layer.

An orthopedic implant must be habitable especially for bone-forming cells (osteoblasts) such that they can colonize on the implant surface and synthesis new bone tissue. Before osteoblasts (or other cells) adhere to an implanted surface, proteins will adsorb from bone marrow, blood and other tissues. In this manner, it has been observed that proteins initially adsorbed onto the surface of implants control subsequent cell adhesion. For this reason, to evaluate the initial protein adsorption events onto the implant material, POM/n-SHA nanocomposite with an area of $1 \times 1\,cm^2$ (each piece) were incubated in the phosphate buffered saline (PBS, pH 7.4) solution containing 10% fetal bovine serum albumin (BSA). Before the incubation process, specimens were treated by ethanol for 30 min and then washed by PBS under gentle shaking for 3 h. Each specimen was then placed in a 24 well culture plate, and 1.0 ml of the BSA/PBS solution was added into each well. The sample specimens were incubated at 37 °C for a time period of 2 h. The amount of absorbed proteins on the nanocomposites was calculated by subtracting the amount of proteins left in the BSA/PBS solution from the amount of proteins in control BSA/PBS solution treated under the identical incubation process.[13] The surface topography of nanocomposites after protein adsorption was studied using AFM analysis.

Results and Discussion

Nanoparticle Characterization Using ATR-FTIR

Figure 1 shows the FTIR patterns of n-HA, and n-SHA. The broad bands from about $3572\,cm^{-1}$ to $2500\,cm^{-1}$ and $631\,cm^{-1}$ arises from stretching and vibration modes of -OH ions. The sharp peak at $3572\,cm^{-1}$ is assigned to be non hydrogen bonded -OH stretching mode usually hydroxyl group of hydroxyapatite. The $1090\,cm^{-1}$ and about $1034\,cm^{-1}$ band arises from $\nu_3\ PO_4^{3-}$, the $963\,cm^{-1}$ band arises from $\nu_1\ PO_4^{3-}$, the $603\,cm^{-1}$ and $565\,cm^{-1}$ band arises from $\nu_4\ PO_4^{3-}$ and $472\,cm^{-1}$ band arises from $\nu_2\ PO_4^{3-}$. The group of weak intense bands in the $2077\,cm^{-1}$and $2003\,cm^{-1}$ region arises from the overtone and combination of ν_3 and ν_1 PO_4^{3-} modes. The bands at about $1411\,cm^{-1}$ and $1448\,cm^{-1}$ in the spectra of HA are attributed to component of the ν_1 mode of CO_3^{2-}.[14] In n-SHA, the new band at $1549\,cm^{-1}$ is ascribed to antisymmetric stretching vibration of COOCa from the interaction between COOH and Ca^{2+}, and the one at $879\,cm^{-1}$ assigned to HPO_4^{2-} group coming from reaction of PO_4^{3-} with H^+ from COOH group. The new absorption bands at 2924, 2854 are due to CH_3 and CH_2 groups coming from stearic acid molecule.

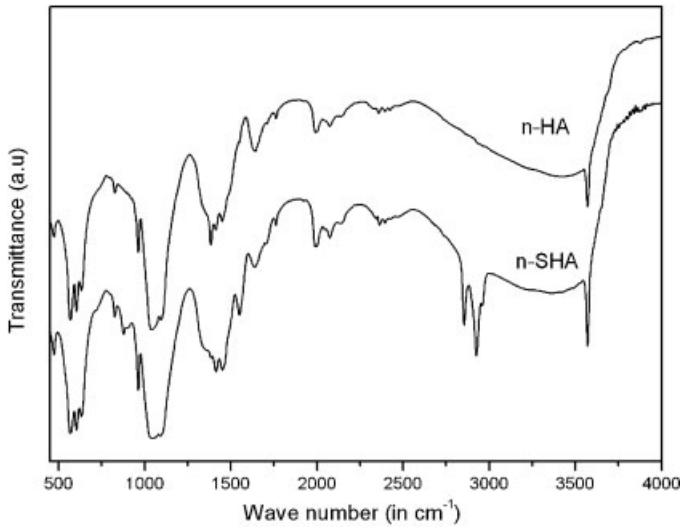

Figure 1.
FTIR patterns of n-HA and n-SHA.

Nanoparticle Characterization Using XRD

The XRD patterns of n-HA and n-SHA are shown in Figure 2. The sharp XRD peaks at 27.3°, 28.63°, 31.96°, 33.23°, 34.30°, 40.22°, 44.23°, 46.70°, and 52.72° indicates the well crystalline phase of HA, which are consistent with the JCPDS data (card number 09 0432). The pure crystalline phase of HA is confirmed by the absence of other forms such as $Ca(OH)_2$, CaO, β-tricalcium phosphate and α-tricalcium phosphate in the XRD patterns. The insignificant decrease in

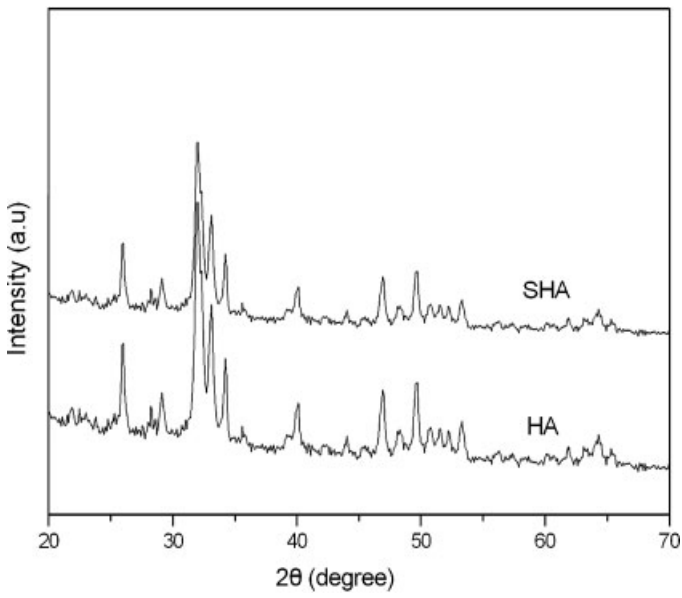

Figure 2.
XRD patterns of n-HA and n-SHA.

the intensity of n-SHA is attributed to the decrease in crystallinity by the organomodification of HA using Sa.

Nanoparticle Characterization Using Transmission Electron Microscopy

The TEM images of the n-HA and n-SHA dispersed in alcoholic medium are shown in Figure 3. It shows that the nanoparticles have rod like structure with about 50–70 nm in length and 20–30 nm in width. The dispersion of HA nanoparticles after modification is obviously better than that before modification. Hence, improved compatibility is expected between n-SHA filler and POM matrix.

AFM Images of the Nanocomposites

AFM is used to understand the nanofiller dispersion in the polymer matrix which distinguishes filler aggregates and single filler particles in the polymer matrix with the surface morphology. In Figure 4 (a-d), the phase images of the composites with filler concentration 0, 1, 3 and 5% are given. Figure 4 a shows the phase image of the neat matrix. As seen in the figure the neat POM surface is smooth and homogenous. In the images of filled nanocomposites, discrete particles embedded in the polymer matrix are seen. The nanocomposites with 1% and 3% loading clearly show more individualized and uniform distribution of filler without any remarkable agglomeration. When the filler content reached 5%, many aggregates on a micrometer scale were observed on the surface of the nanocomposites.

The surface roughness of bone implant has a significant influence on the adhesion and proliferation of osteoblasts.[15] The changes in the surface topography of nanocomposite could be determined quantitatively in terms of surface parameters, such as the average roughness, R_a and the root mean square (RMS) roughness, R_q.[16] The R_q and R_a values of composites are given in Table 1. In case of the neat POM, R_q value was found to be 3.99 nm and R_a was 3.52 nm. Generally, R_q and R_a values will be almost equal, if there is no large deviation from the mean surface level. The difference between R_q and R_a value of 0.47 nm suggests that there is not much undulation for neat matrix. It can be seen that all the nanocomposites show higher (R_q - R_a) values compared to that of neat polymer, which confirms the presence of filler particles on the surface. It was found that roughness parameters increase with filler loading and show maximum value at 5%. When the amount of fillers is augmented to a certain extent the high viscosity of casting solution and lot directional - aligned filler grains existing on the surface may result in a rapid increase of surface roughness. Since natural bone has a nano rough surface consisting of nanosized hydroxyapatite and collagen molecules, producing nano rough surfaces on these implants is more favorable for early osteoblast adhesion and growth on nanocomposite surface,

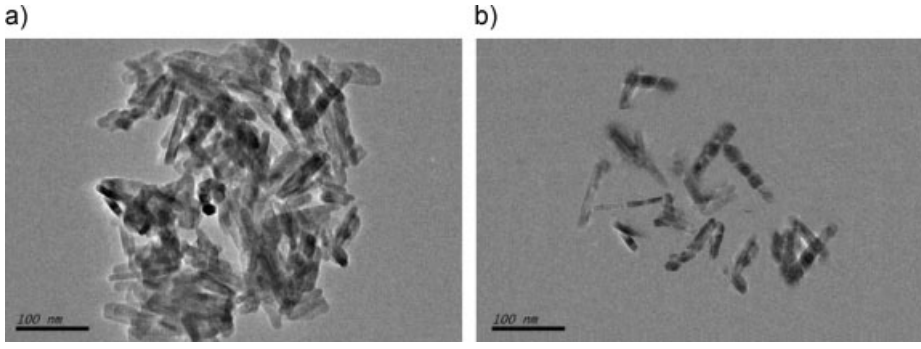

Figure 3.
TEM images of the n-HA and n-SHA.

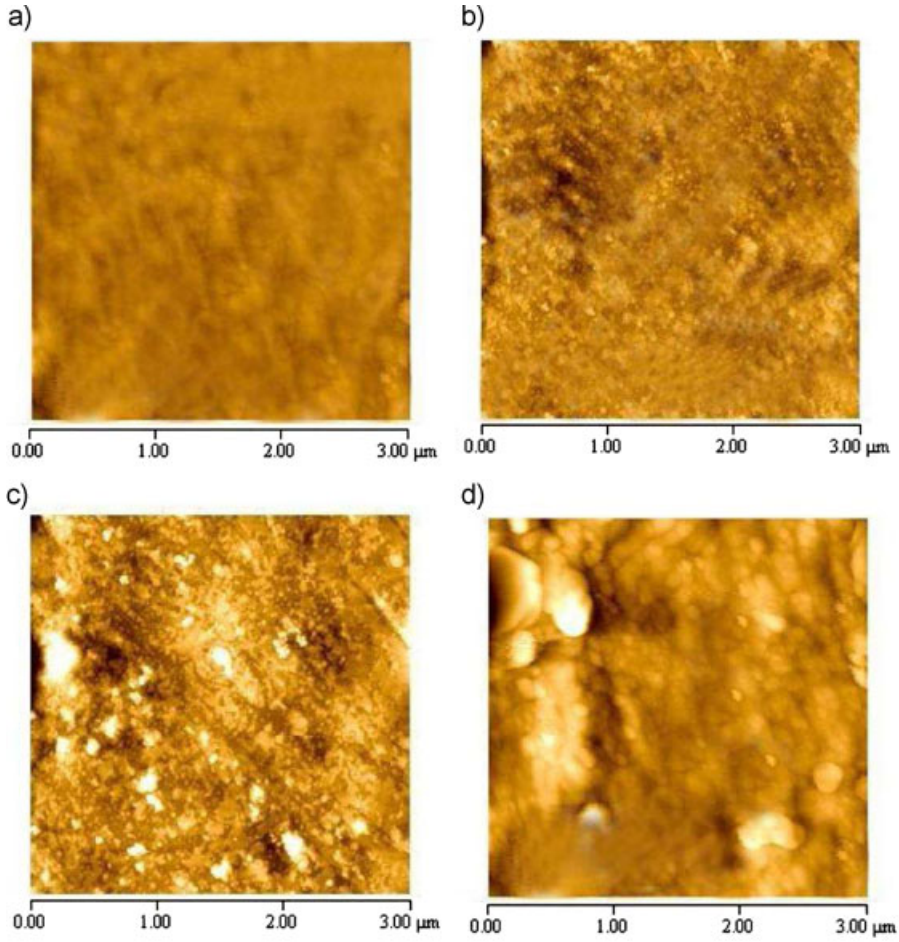

Figure 4.
AFM images of POM nanocomposites: (a) POM, (b) POM1, (c) POM3, and (d) POM5.

which improves orthopedic implant efficacy.[17] Therefore the use of the substrate with higher roughness provides coatings with better adhesion on the substrate, proper to biomedical applications.

Table 1.
Roughness parameters of the nanocomposites.

Nanocomposites	R_q (nm)	R_a (nm)	R_q - R_a (nm)
POM	3.99	3.52	0.47
POM1	5.13	3.04	2.09
POM3	8.18	5.29	2.89
POM5	11.21	7.80	3.41

Mechanical Properties

The mechanical properties of nano-ceramic/polymer composites depend strongly on the size and shape of ceramic nanoparticles, dispersion of nanoparticles, particle loading, interfacial adhesion between the ceramic and polymer phase, and inherent properties of the polymer matrix. So the change in these properties with varying filler content can be taken as an alternative method to evaluate the dispersion of nanofiller in the polymer matrix.[18]

The mechanical properties of the POM nanocomposites with varying filler content were characterized by tensile tests, and thus

Table 2.
Mechanical properties of POM/n-SHA nanocomposites.

Sample	Tensile strength (MPa)	Young's modulus (MPa)	Elongation at break (%)
POM	55.35(0.2)	690.00(0.3)	17(0.8)
POM1	58.55(0.1)	694.66(0.2)	18(1.2)
POM3	63.45(0.1)	697.67(0.1)	20(0.7)
POM5	59.05(0.1)	700.07(0.4)	19(0.8)

Numbers in the parenthesis are standard deviation.

tensile strength, elongation at break and Young's modulus were calculated. From Table 2, it can be seen that mechanical properties like tensile strength and elongation at break of nanocomposites show a tendency to increase and then decrease with increasing *n*-SHA content and have maximum value at 3% filler content. The highest value of tensile strength and elongation at break obtained for the nanocomposite with 3% of filler loading is due to the good dispersion and the improved interfacial adhesion between nanofillers and POM matrix, which results in the effective transfer of applied stress to the particles from the matrix. The more uniform the nanoparticle dispersion in the polymer and the stronger interaction between the nanoparticles and polymer matrix, the more improved the mechanical properties.[19] The potential explanation for the decrease in the tensile strength after optimum filler content (3%) is mainly due to the agglomeration of n-SHA particles, which was evidenced from the morphological analyses. In 5% nanocomposite, discontinuity in the form of debonding exists because of non-adherence of nanofillers to the polymer and the stress transfer at the polymer/n-SHA particles interface becomes ineffective.[20]

Tensile modulus, expressing the stiffness of the material, is a bulk property that depends primarily on the geometry, particle size distribution and concentration of the filler. The exact nature of the tensile response of a polymeric material depends upon the chemical structure of the polymer, conditions of the sample preparation, molecular weight, molecular weight distribution, and the extend of any cross linking or branching. Tensile modulus show noticeable improvement, with addition of nanofiller to POM. It is well known that the modulus increases for a polymer when we incorporate any mineral filler into it. This is reasonable because the rigid inorganic fillers have higher stiffness values than the organic polymer.[21,22] The ability of nanocomposites to tailor the mechanical strength by varying the filler content makes it a better candidate material for more effective orthopedic applications from a mechanical perspective.

Contact Angle Studies

Contact angle measurements carried out with water are often used as an empirical indicator of wettability of POM/n-SHA nanocomposites. The contact angle of pure POM was 75°. With the addition of 1, 3 and 5 wt% nanofiller, the contact angles increased to 78, 81 and 82.7° respectively, which indicate that the presence of n-SHA in the POM matrix improves the hydrophobicity of the nanocomposite surfaces.

The increase in hydrophobicity is mainly attributed to the difference in both the chemical composition of the polymer surface and its surface morphology. In order to have a homogenous dispersion in hydrophobic polymeric host, n-HA surface was modified with Sa, which lowers the hydrophilicity of filler surface and impart hydrophobic characteristics to the surface of n-HA.[23] In a multi-component system, the difference in the surface energy of components results in a relative enrichment of the lower-surface-energy material at the air interface. The placement of lower surface energy component at the surface, for maintaining a gradient between the surface and bulk composition, lowers the equilibrium surface energy.[24] So, in the POM

nanocomposite system, lower surface energy n-SHA components migrate to the surface due to the difference in the surface energy of the components. Thus, the nanocomposite surfaces become more hydrophobic relative to the neat polymer due to the formation surface with lower equilibrium surface energy. The correlation between AFM surface analysis and water contact angle measurements indicated that the increase in surface roughness increases the hydrophobicity by increasing the surface area.[25] These results reveal that the addition of n-SHA can increase the hydrophobic nature of the POM which plays a critical role in the cell- implant interaction either directly by the controlling adsorption of proteins present in the cell culture medium or by guiding cell spreading with suitable topography.[26]

Thermogravimetric Analysis

In order to determine the thermal stability of POM nanocomposites with different nanofiller content (0, 1, 3, and 5%), thermal behavior of the nanocomposites were analyzed using TGA and the resultant thermo grams are shown in Figure 5. The incorporation of n-SHA into POM matrix slightly increased the thermal decomposition temperatures and the char yields of POM nanocomposites. The presence of n-SHA could lead to the stabilization of POM matrix, resulting in the increase of the thermal stability of POM nanocomposites. The introduced POM could induce protective barriers against thermal decomposition and retard the thermal decomposition of POM nanocomposites, resulting from the effective function of n-SHA acting as physical barriers to hinder the transport of volatile decomposed products out of POM nanocomposites during thermal decomposition.[27] The similar trend was reported for nanocomposites in which stearic acid modified calcium carbonate nanoparticles were used as nanofillers in the polymer matrix.[28] Based on these studies, it is clear that thermal degradation is not a concern during sterilization prior to the clinical use of POM nanocomposite biomaterials around 37 °C.

Biocompatibility Studies

Simulated Body Fluid Test

Bioactivity of orthopedic materials was widely investigated by SBF immersion experiments, because such in vitro evaluation was simple and efficient, and has been demonstrated fair correlation with in vivo test. Therefore, the apatite forming ability of the POM nanocomposite implants was

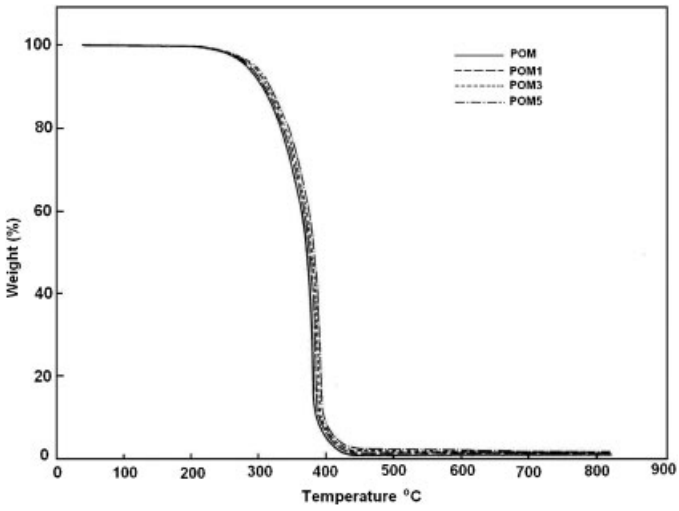

Figure 5.
Thermogravimetric curves of POM/n-SHA nanocomposites.

studied by soaking in SBF that mimics the electrolyte content of human blood plasma. AFM images of nanocomposites after soaking in SBF for 7 days are presented in Figure 6. This allows the comparison of apatite formation on the nanocomposites surfaces with varying filler concentration before and after soaking in SBF. The white deposits on the surfaces confirm the formation of apatite layer. In the case of unfilled samples, some scattered and discrete deposits were seen on the surface. But in nanocomposites, the deposition increased with the increasing filler content. When the filler content reached 5%, these deposits cover the entire nanocomposite surface and large aggregated deposits were found at different areas of the composite surface, which is not in the case of nanocomposites with low filler content. This suggests that the large deposits might have been formed by a secondary nucleation mechanism onto nanosized calcium phosphate entities initially formed. The nucleation of apatite should be easier on a surface of the same nature (apatite) compared to the nucleation on a chemically different surface. Even the surface roughness has no pronounce effect

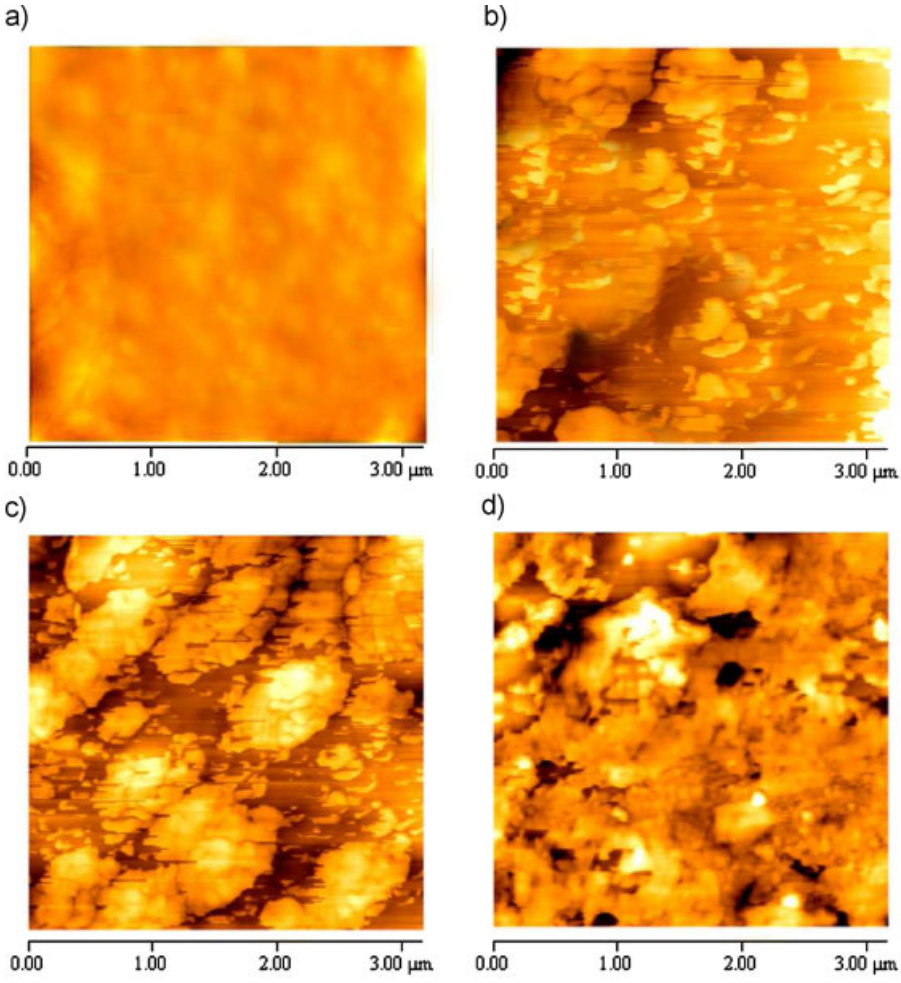

Figure 6.
AFM images showing the formation of apatite layer on the surface of POM nanocomposites after 7 days SBF immersion: (a) POM; (b) POM1; (c) POM3; and (d) POM5.

on the initial heterogeneous nucleation of apatite, rough topography of 5% nanocomposite is beneficial for the further growth and mechanical attachment of apatite coating on the implant surface.[29]

The mechanism for the nucleation and growth of apatite on the implant surface was proposed by Hench et al.[30,31] The exchange of H_3O^+ from the SBF solution with Ca in the nano hydroxyapatite fillers on the nanocomposite surface gives rise to the formation of Si-OH groups and leaves behind a silica-rich leached layer. The formation of apatite is closely related to the amount of Si-OH groups present on the surface of bioactive materials, since Si-OH groups are proposed to provide specific favorable sites for the apatite nucleation. The high surface area of the nanofillers on the implant surface facilitates the exchange of Ca^{2+} in hydroxyapatite with H_3O^+ from the SBF solution and lead to higher density of Si-OH groups on the surface, which results in the higher apatite nucleation rate with increasing filler content. Once the apatite nuclei are formed, they grow spontaneously by the transport of Ca^{2+}, HPO_4^{2-}, OH^-, and CO_3^{2-} species from the SBF solution to the nuclei and the fast deposition of apatite. From this it is well evidenced that n-SHA introduced not only acts as reinforcing fillers, but also provides a bioactive character to the nanocomposite.

Protein Adsorption Studies

The proteins adsorbed on a biomaterial surface after implantation largely govern the biocompatibility and host response of the implant biomaterial. Protein adsorption in a polymer nanocomposite surface starts with a monolayer formation by the interaction between the nanocomposite surface and proteins and subsequent layers are formed by the disulfide linkages between the monolayer proteins in the surface and proteins in the bulk solutions. The structure of the monolayer formed on the surface has profound effect on the interaction of cells with the implant and is largely governed by the chemistry and morphology of the polymer surface.[32] So in order to evaluate implant's potential towards cell adhesion applications, it is important to understand how the nanostructure of the implant will affect the initial protein adsorption. As shown in Figure 7, the protein adhesion capacity of nanocomposites increased with increase in the filler content.

This improved protein adhesion capacity of nanocomposites is due to the increased

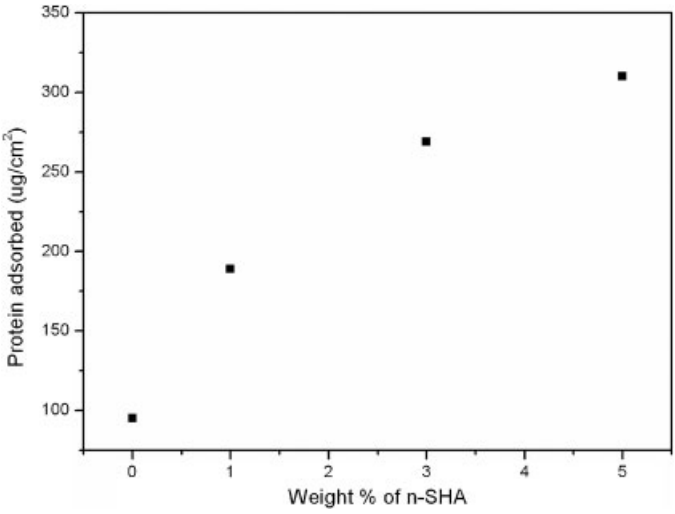

Figure 7.
Dependency of protein adsorption on the amount of n-SHA in nanocomposites.

surface area and nanoscale surface features of n-SHA which provides more available sites for protein adsorption. The hydrophobic interaction between the protein and implant surface is maximum in nanocomposites compared to pure POM because of the presence of hydrophobic n-SHA which maximizes the interfacial free energy. Thus, as the content of n-SHA increases, more n-SHA crystals could be exposed on the POM nanocomposite surfaces to lowers the surface energy of the system, which resulted in improved protein adsorption capacity. The non polar surfaces destabilize proteins and thereby facilitate conformational reorientations leading a strong inter protein and protein-surface interactions.[33]

Topographical AFM images of POM nanocomposites after protein adsorption are depicted in Figure 8. The presence of BSA molecules on implant surface is confirmed from the spherical features seen on the surface after BSA addition. The thickness of the layer denotes the amount of adsorbed BSA and the comparison between the images revealed that extend of adsorption increases with filler content. The positive correlation between extent of protein adsorption and the hydrophobicity of nanocomposite surface suggest that the hydro-

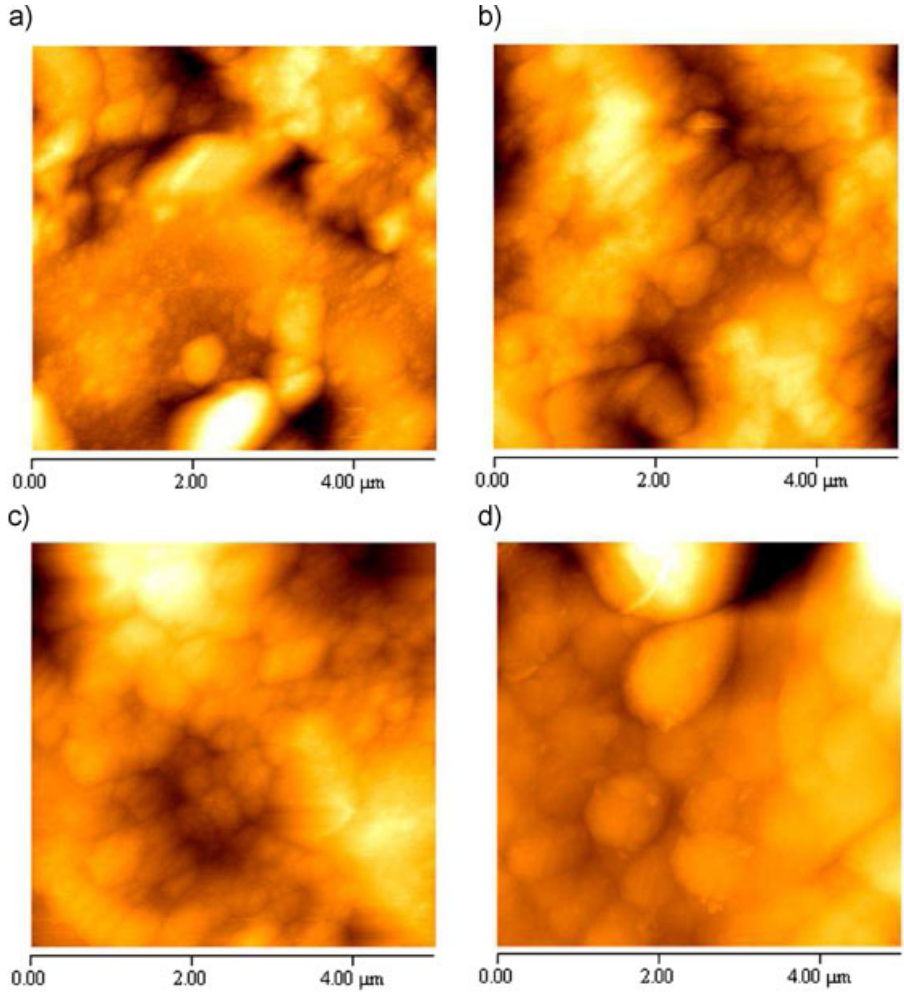

Figure 8.
AFM images of POM nanocomposites after protein adsorption (a) POM, (b) POM1, (c) POM3, (d) POM5.

phobic interaction is a major driving force for adsorption. Proteins tend to adsorbs more extensively and less reversibly at hydrophobic surfaces than at hydrophilic surfaces. With increasing degree of hydrophobicity of the surface, the ease of exchange of adsorbed protein molecules with the bulk aqueous phase is generally reduced. This difference can be attributed to a greater degree of unfolding at hydrophobic surfaces following instantaneous protein adsorption, which leads to the development of strong interfacial hydrophobic interactions and associated displacement of vicinal water molecules from the unfavorable environment of the surface. This explains the rather general experimental finding that in most cases the affinity of proteins to surfaces increases on hydrophobic substrates and decreases on hydrophilic substrates.[34] Further, increased adsorption with filler content is also related to its high surface roughness and increase in roughness favors the protein to transport preferentially to valleys on the nanocomposite surface.[35] However, the uniform distribution in the nanocomposites minimizes the bilateral disulphide bond formation among the protein molecules and which leads to the more aligned cake layer protein on the surface.[36] The results from these experiments serve as a guide to tune protein adsorption behavior of polymer nanocomposite surface as a function of filler composition and to understand the role of nanomorphology in cell polymer nanocomposite interactions.

Conclusion

POM nanocomposites with variable amounts of stearic acid modified nano hydroxyapatite were prepared by melt mixing and mechanical, thermal, hydrophobic and biocompatible properties were investigated. AFM measurements showed the presence of filler particles on the surface of nanocomposites which caused the increase in (R_q - R_a) values compared to the virgin polymer. The mechanical properties of the nanocomposites like tensile strength and elongation at break showed improvements at lower filler content and decreased with higher filler loading while Young's modulus showed increase with respect to the loading. The hydrophobic properties of polymer nanocomposites were enhanced by the incorporation of *n*-SHA, as evidenced by increased contact angle. The nanocomposites induced a dense and continuous layer of apatite, after soaking them in simulated body fluid (SBF) for 1 week. The increased surface area and nanoscale surface features of nanomaterials provide more available sites for protein adsorption on the nanocomposite surface with increasing filler content. Thus the high performance POM/hydroxyapatite nanocomposites with excellent mechanical and bioactive properties developed under this study can be used as a low cost attractive alternative for the expensive bone replacement treatment.

Acknowledgements: Ajith James Jose acknowledges the scholarship grant in 'National Doctoral Fellowship' category by All India Council for Technical Education, New Delhi, India.

[1] M. Wang, *Biomaterials* **2003**, *24*, 2133.
[2] R. Murugan, S. Ramakrishna, *Compos. Sci. Technol.* **2005**, *65*, 2385.
[3] S. Raynaud, E. Champion, D. B. Assollant, P. Thomas, *Biomaterials* **2002**, *23*, 1065.
[4] S. M. Best, A. E. Porter, E. S. Thian, J. Huang, *J. Eur. Ceram. Soc.* **2008**, *28*, 1319.
[5] K. Pielichowska, *Int. J. Mater. Form.* **2008**, *1*, 941.
[6] A. Ohlin, L. Linder, *Biomaterials.* **1993**, *14*, 288.
[7] L. Eschbach, *Int. J. Care Injured*, **2000**, *31*, 22.
[8] H. Liu, T. J. Webster, *Biomaterials* **2007**, *28*, 354.
[9] P. Tran, T. J. Webster, *Int. J. Nanomed.* **2008**, *3*, 391.
[10] Y. Li, W. Weng, *J. Mater. Sci: Mater Med.* **2008**, *19*, 19.
[11] A. J. Jose, M. Alagar, *Polym. Compos.* **2011**, *32*, 1315.
[12] T. Kokubo, H. Takadama, *Biomaterials*, **2006**, *27*, 2907.
[13] H. Lee, S. E. Kim, H. W. Choi, C. W. Kim, K. J. Kim, S. C. Lee, *Eur. Polym. J.* **2007**, *43*, 1602.
[14] . Elliot, D. W. Holcomb, R. A. Young, *Calcif. Tissue Int.* **1985**, *37*, 275.
[15] V. Nelea, C. Morosanu, M. Iliescu, I. N. Mihailescu, *Appl. Surf. Sci.* **2004**, *228*, 346.

[16] A. J. Jose, M. Alagar, A. S. Aprem, *Int. J. Polym. Mater.* **2012**, *61*, 544.
[17] M. Sato, T. J. Webster, *Expert Rev. Med. Devices.* **2004**, *1*, 105.
[18] H. Liu, T. J. Webster, *Int. J. Nanomed.* **2010**, *5*, 299.
[19] A. S. Luyt, M. D. Dramic anin, Z. Antic, V. Djokovic, *Polym. Test.* **2009**, *28*, 348.
[20] A. J. Jose, M. Alagar, S. P. Thomas, *Mater. Manuf. Processes.* **2012**, *3*, 247.
[21] S. Fu, X. Feng, B. Lauke, Y. Mai, *Composites: Part B*, **2008**, *39*, 933.
[22] S. P. Thomas, S. Thomas, S. Bandyopadhyay, *J. Phys. Chem.* **2009**, *113*, 97.
[23] Y. H. Lai, M. C. Kuo, J. C. Huang, M. Chen, *Mater. Sci. Eng. A* . **2007**,*458*, 158.
[24] M. Lewin, *Fire Mater.* **2003**, *27*, 1.
[25] M. Khayet, C. Y. T. Feng, *J. Membr. Sci.* **2003**, *213*, 159.
[26] L. D. Bartolo, S. Morelli, A. Bader, E. Drioli, *J. Mater. Sci. - Mater. Med.* **2001**, *12*, 959.
[27] H. Zou, S. Wu, J. Shen, *Chem. Rev.* **2008**, *108*, 3893.
[28] W. Wang, X. Zeng, G. Wang, J. F. Chen, *J. Appl. Polym. Sci.* **2007**, *106*, 1932.
[29] F. Barrere, M. E. Margot, . Snel, A. Clemens, V. Blitterswijk, K. Groot, P. Layrolle, *Biomaterials* **2004**, *25*, 2901.
[30] J. M. Raquez, D. T. J. Barone, Z. Luklinska, O. Persenaire, A. Belayew, J. Eyckmans, J. Schrooten, P. Dubois, *Biomacromolecules*, **2011**, *12*, 692.
[31] O. Rodrige, C. Arthur, W. Jon, B. Anthony, L. Hench, *J. Biomed. Mater. Res. Part A*, **2007**, *80*, 565.
[32] M. Palacio, S. Schricker, B. Bhushan, *J. Microsc.* **2010**, *240*, 239.
[33] J. Yoon, J. H. Kim, W. S. Kim, *Colloids Surf., A* **1999**, *153*, 413.
[34] R. D. Tilton, C. R. Robertson, A. P. Gast, *Langmuir* **1991**, *7*, 2710.
[35] L. Hao, J. Lawrence, *Colloids Surf., B.* **2004**, *34*, 87.
[36] M. Rabe, D. Verdes, S. Seeger, *Adv. Colloid Interface Sci.* **2011**, *162*, 87.

